Amplitude Symmetry Detection for Interfering Signals in CNC Satellite Communications

Habib Alizadeh[1], Mohsen Rezaee[2], Morteza Babaei[3]

1- PhD Candidate Faculty of Electrical Engineering Department, Imam Hossein University, Tehran, Iran.
Email: habib.alizadeh@ihu.ac.ir

2- Assistant Professor ICT Research Institute, Tehran, Iran.
Email: m.rezaeekh@itrc.ac.ir (Corresponding Author)

3- Assistant Professor Faculty of Electrical Engineering Department, Imam Hossein University, Tehran, Iran.
Email: mbabaei @ihu.ac.ir

Received: 11 June 2023 Revised: 29 July 2023 Accepted: 13 August 2023

ABSTRACT:
Satellite communications technology developed rapidly and plays important role in communication networks. In the meantime, CNC satellite communication has received much attention due to its high spectral efficiency. However, the analysis of this type of communication signal in non-cooperative receivers is associated with many challenges due to the nature of time-frequency overlap. The proposed methods in this field have been developed assuming either symmetry or asymmetry in the amplitude of the two interfering signals. However, a reliable method to detect the amplitude symmetry in the non-cooperative receivers is missing in the literature. Thus, in this article, the symmetry or asymmetry of the amplitude of time-frequency overlapping signals of these type of communications has been analyzed using higher-order statistics. For this purpose, the mathematical relationships of higher-order statistics for the model of time-frequency interfering signals received in the non-cooperative receiver have been developed. Then, the appropriate decision function is defined based on different ratios of higher-order statistics of the received signal. This decision function is used to detect amplitude symmetry or asymmetry in time-frequency overlapping signals for CNC communication. The simulations show that the decision-making function based on the sixth and fourth ratio cumulants is a reliable metric, such that the probability of correct classification at signal-to-noise levels higher than 25dB for BPSK modulation is more than 80%, and for QPSK modulation is more than 90%.

KEYWORDS: CNC satellite Communication, High-Order Statistics, Symmetric CNC.

1. INTRODUCTION

Carrier-in-Carrier (CNC) is advanced satellite communication technology [1]. The signals sent by two earth stations are overlapped both in time and frequency domains. Hance, the required bandwidth can be reduced up to 50%. In a conventional satellite communication links that uses Frequency Division Multiplexing (FDM) or Single Channel Per-Carrier (SCPC), two different carrier frequencies are used in disparate bandwidths for sending and receiving. In this case, the carrier frequencies do not overlap. But CNC technology, using signal processing algorithm and a technique called adaptive cancellation, makes it possible to use the same bandwidth for transmission and reception, allowing two carriers to be placed on the same center frequency, which is impossible for conventional transmission and reception methods. This issue is shown in the comparison of Figure s 1 and 2.

So, the problem is the analysis of satellite communications signals based on CNC technology in non-cooperative receivers. Because the signal received from the downlink of CNC satellite communication has the nature of time and frequency overlapping, the non-cooperative receiver cannot use the previous information in the signal separation process like the cooperating receivers [4]. Therefore, signals analysis is still considered an important and complicated issue.

If interfering time-frequency signals have the same modulation, based on the amplitude difference of these signals, the separation problem can be divided into two categories, symmetric and asymmetric. In symmetrical mode, the two satellite communication stations share the same channel, and the amplitude of the two signals is equal, while in asymmetrical mode, the amplitude of two signals differ greatly [5].

Paper type: Research paper
DOI: 10.30486/mjtd.2023.1988534.1037
How to cite this paper: H. Alizadeh, M. Rezaee and M. Babaei, "**Amplitude Symmetry Detection for Interfering Signals in CNC Satellite Communications**", *Majlesi Journal of Telecommunication Devices*, Vol. 12, No.3, pp.149-159, 2023.

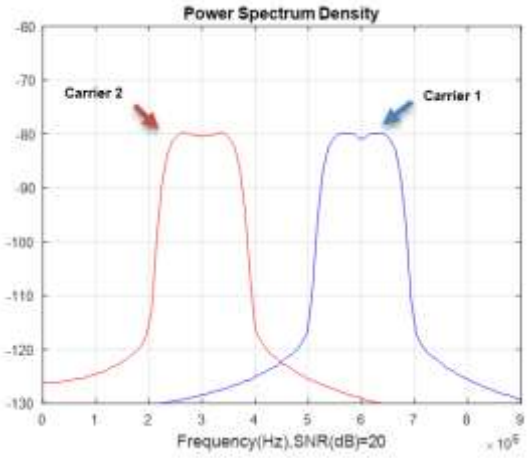

Fig. 1. Two-way satellite communication by SCPC [3].

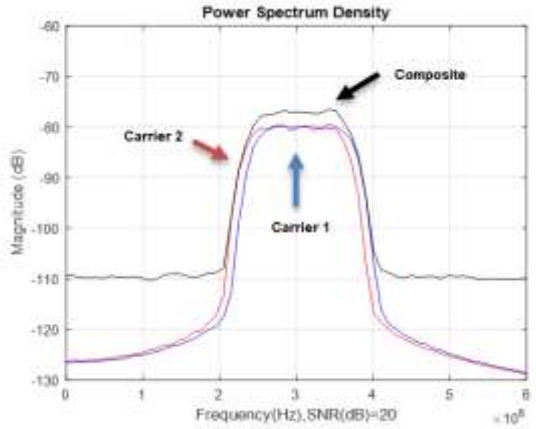

Fig. 2. Two-way satellite communication by CNC technology [3].

The importance of identifying symmetry or asymmetry in these interfering signals is due to the difference in separation methods and their complexity. The separation in asymmetric mode is easier due to the existence of this amplitude difference. So, in [6], [7], and [8] the amplitude asymmetry of interfering signals is used to separate the signals. In [9], amplitude asymmetry of the interfering signals is used to estimate the frequency offset. [5] took advantage of the existing symmetry in the signal domain to separate CNC time-frequency overlapping signals using an improved quantum-inspired evolutionary algorithm. It has been shown in [10] that the proposed algorithms are suiTable for the symmetric mode and the efficiency of the proposed method decreases with the increase of the amplitude difference of interfering signals. However, researchers have not provided an approach to distinguish between symmetric and asymmetric modes.

Higher-order statistics such as cumulants and moments of the modulated signals have been studied extensively. cumulants and moments, are especially popular as features of interest in received communication signal. Among them, the signal statistics-based feature, especially the Higher-Order Cumulants (HOC), owing to its inherent immunity to gaussian noise. For this purpose, in this article, higher-order statistics are used to define the decision function regarding the detection of amplitude symmetry or asymmetry. Therefore, in section 2, the time-frequency interfering signal received at the non-cooperative receiver is mathematically modeled, and based on this model, the concept of amplitude symmetry is explained. Then, in section 3, the theoretical foundation of higher-order statisticians will be examined, and in section 4, the cumulants relations will be developed based on the mathematical model of interfering signals in non-cooperative receivers. In section 5, higher-order even cumulants ratios are used to define the decision function, and finally, in section 6, cumulants ratios are compared and evaluated with simulated data.

2. MATHEMATICAL MODELING OF CNC SATELLITE COMMUNICATIONS IN NON-COOPERATIVE RECEIVER AND THE CONCEPT OF AMPLITUDE SYMMETRY

In this section, the time-frequency interfering signals of CNC communications received in the non-cooperative receiver are modeled. If we assume that each of the ground stations sends signals with the same characteristics, then the model of the signal sent from each of the stations and the signal received at the non-cooperating receiver can be shown in Figure 3.

As shown in Figure 3, $C_n^{(1)}$ and $C_n^{(2)}$ are the bit sequences of each ground station. The sequence of bits are modulated into $s_n^{(1)}$ and $s_n^{(2)}$ symbols, respectively. The symbols are sent after passing through the shaping filters. The transmitted signals are received in the satellite transponder after the addition of the uplink channel noise along with the amplitude attenuation, phase offset and frequency offset. Then, after frequency shifting, the transponder sends the signals in a common bandwidth in the downlink channel which is received along with the downlink channel noise in the non-cooperative receiver.

According to Figure 3, the baseband equivalent received signal in the receiver will be a combination of two signals, which can be expressed as

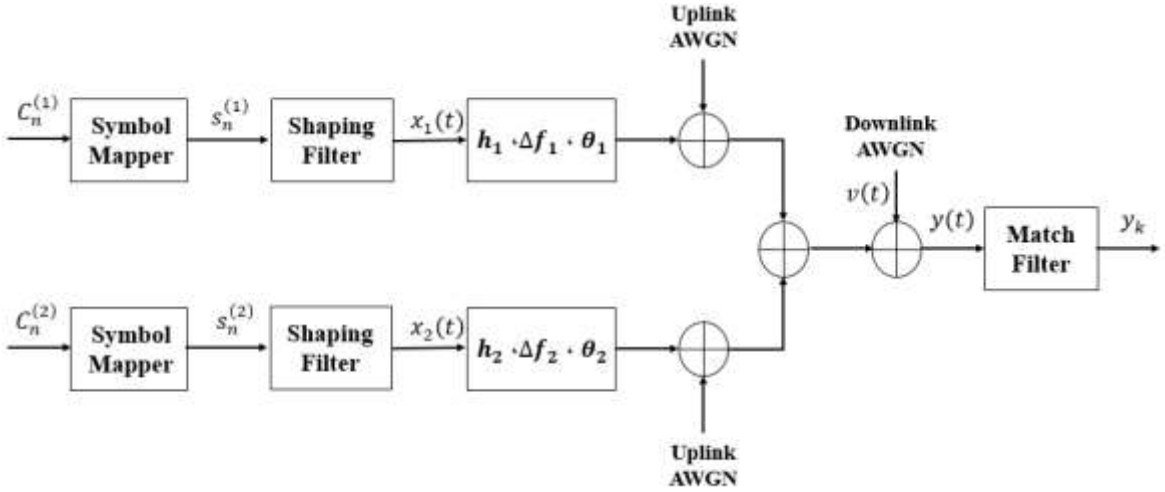

Fig. 3. The model of the signals sent from two stations and the signal received at the non-cooperative receiver.

the path, and $v(t)$ is the additive gaussian white noise. $x_i(t)$ are the transmitted signals defined by Equation 2:

$$x_i(t) = \sum_{n=-\infty}^{+\infty} s_n^{(i)} g_i\big(t - nT + \tau_i(t)\big), i = 1,2 \quad (2)$$

If PSK modulations are used, ،$s_n^{(i)}$ are independent and identically distributed (iid) random variables. The $g_i(t)$ is the pulse shaping filter, assuming that it is in the limited time interval between $-LT$ and LT, ،$0 < \tau_i(t) < T$ is the relative time delay between two modulated signals and T is the duration of one symbol. Here, the pulse shaping filter is defined as

$$g_i(t) = \frac{\cos(\frac{\beta_i \pi t}{T})}{1 - 4(\frac{\beta_i t}{T})^2} \times \frac{\sin(\frac{\pi t}{T})}{\frac{\pi t}{T}} \quad (3)$$

In this relation, β_i for $i = 1,2$ is the roll-off factor of the shaping filter.

If the output signal of the matched filter is sampled at a rate of $1/T$, the discrete-time model of the signal at the non-cooperative receiver is obtained:

$$y_k = h_1 e^{j(2\pi\Delta f_1 kT + \theta_1)} x_k{}^{(1)} + h_2 e^{j(2\pi\Delta f_2 kT + \theta_2)} x_k{}^{(2)} + v_k \quad (4)$$

in which we have $y_k = y(kT)$, $v_k = v(kT)$ and the transmitted signal is rewritten as:

$$x_k{}^{(i)} = x_i(kT) \quad (5)$$

$$= \sum_{n=1-L}^{L} s_{k+n}^{(i)} g_i(-nT + \tau_k{}^{(i)})$$

in which, $\tau_k{}^{(i)} = \tau_i(kT)$ and $k = 0،1، \dots ،K-1$ will be limited in time.

The time-frequency interfering signal received in the non-cooperative receiver can be symmetric or asymmetric. In symmetric mode, all communication specifications and features of the two stations are the same, and the stations use the same hardware equipment and broadcasting conditions to exchange signals [15]. In this case, the power of the received signals in the non-cooperative receiver is the same. In other words, interfering signals will have amplitude symmetry if the following relationship holds:

$$h_1 \approx h_2 \quad (6)$$

Figure 2 is a representation of communication with amplitude symmetry, where the power level of the interfering signals in the first and second carriers are equal. If the stations are using different modulations, hardware equipment, or broadcasting conditions in their communication, it will cause the power level of the two stations to be different and h_1 and h_2 in the non-cooperative receiver will be different as shown in Figure 4.

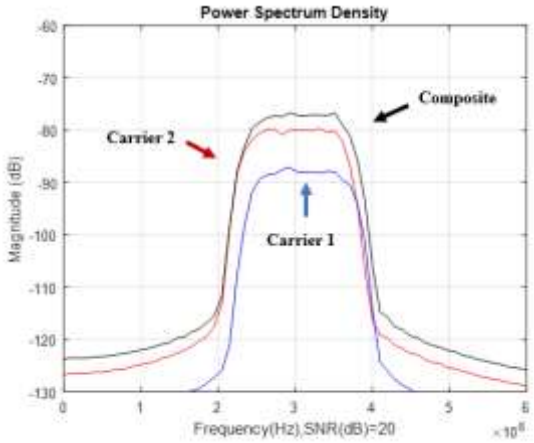

Fig. 4. Asymmetric CNC satellite two-way communication.

3. THE THEORETICAL FOUNDATION OF HIGHER-ORDER CUMULANTS

Higher-order cumulants characterize the shape of the distribution of the noisy baseband samples and have a natural robustness to constellation rotation and phase jitter [17]. So, in [16], [18], higher-order cumulants are used as a feature-based method in modulation classification. Before defining the cumulant, the moment must be described first.

The moment of the zero mean random signal y of order p with q conjugate is defined as the following relationship [18]:

$$M_{pq} = \mathrm{E}\{\mathrm{y}^{p-q}\mathrm{y}^{*q}\} \tag{7}$$

So, the cumulant of order p with q conjugate is defined as follows [18]:

$$C_{pq} = \mathrm{Cum}\{\underbrace{\mathrm{y}, \dots, \mathrm{y}}_{p-q}\,\underbrace{\mathrm{y}^*, \dots, y^*}_{q}\} \tag{8}$$

Of course, cumulants can be defined in terms of moments in the following relation [18]:

$$\mathrm{Cum}\{y_1, y_2, \dots, y_p\} = \sum_{\psi}(\eta-1)!\,(-1)^{\eta-1}\prod_{\phi\in\psi}E\{\prod_{i\in\phi}y_i\} \tag{9}$$

where ψ includes all partitions 1, 2, … , p and ϕ the list of all blocks of the partition ψ. The number of elements in the expression ϕ is denoted by η. Since the computational complexity increases with the cumulant order, in this article cumulants of up to order sixth are used, which are defined in terms of moments in the Table 1 [19].

Table 1. Higher-order cumulants and higher-order moments [19].

HOCs		HOMs
Second Order Cumulants	C_{20}	M_{20}
	C_{21}	M_{21}
Fourth Order Cumulants	C_{40}	$M_{41} - 3{M_{20}}^2$
	C_{41}	$M_{40} - 3M_{20}M_{21}$
	C_{42}	$M_{42} - \lvert M_{20}\rvert^2 - 2{M_{21}}^2$
Sixth Order Cumulants	C_{60}	$M_{60} - 15M_{20}M_{40} + 30{M_{20}}^3$
	C_{61}	$M_{61} - 5M_{21}M_{40} - 10M_{20}M_{41} + 30{M_{20}}^2M_{21}$
	C_{62}	$M_{62} - 6M_{20}M_{42} - 8M_{21}M_{41} - M_{22}M_{40} + 6{M_{20}}^2M_{22} + 24{M_{21}}^2M_{20}$
	C_{63}	$M_{63} - 9M_{21}M_{42} + 12\lvert M_{20}\rvert^2M_{21} + 12{M_{21}}^3$

In practice, the theoretical values of higher-order moments are estimated using a long sequence of N samples of the received signal as follows:

$$\widehat{M}_{pq} = \frac{1}{N}\sum_{k=1}^{N}{y_k}^{p-q}{y_k}^{*q} \tag{10}$$

Using the results of this estimation and Table 1, higher-order cumulants can also be estimated. BPSK and QPSK modulations are widely used in CNC satellite communications, and the theoretical values of the higher-order normalized moments of these modulations are shown in Table 2 [18].

Table 2. - Higher order normalized moments of BPSK and QPSK modulation [18].

	BPSK	QPSK
M_{20}	1	0
M_{21}	1	1
M_{40}	1	1
M_{41}	1	0
M_{42}	1	1
M_{60}	1	0
M_{61}	1	1
M_{62}	1	0
M_{63}	1	1

Using the values of the moments in Table 2, the higher-order cumulants of two modulations are estimated using the mathematical relationships in Table 1 in the form of Table 3 [18], [20].

Table 3. Higher-order cumulants of BPSK and QPSK modulation [18] and [20].

	BPSK	QPSK
C_{20}	1	0
C_{21}	1	1
C_{40}	-2	1
C_{41}	-2	0
C_{42}	-2	-1
C_{60}	16	0
C_{61}	16	-4
C_{62}	16	0
C_{63}	16	4

The results of theoretical values in the Table 3 will be used to define the decision function. Before that, the cumulant of the time-frequency interfering signals received in the non-cooperative receiver must be calculated.

4. HIGHER-ORDER CUMULANT OF TIME-FREQUENCY INTERFERING SIGNALS

If we assume that X and Y are statistically independent random variables, the cumulant of their sum is separated as follows [21]:

$$C_{pq}(\alpha X + \beta Y) = \alpha^{p-q}\alpha^{*q}C_{pq}(X) + \beta^{p-q}\beta^{*q}C_{pq}(Y) \quad (11)$$

where α and β are complex constant coefficients. This feature can be used to develop higher-order cumulants on the mathematical model of Equation 3. Therefore, the cumulant of order p with q conjugate of the time-frequency interfering signal received in the non-cooperative receiver will be separated as follows:

$$C_{pq}(y_k) = h_1^p C_{pq}(e^{j(p-2q)(2\pi\Delta f_1 kT+\theta_1)}{x_k}^{(1)}) + h_2^p C_{pq}(e^{j(p-2q)(2\pi\Delta f_2 kT+\theta_2)}{x_k}^{(2)}) + C_{pq}(v_k) \quad (12)$$

Since the higher-order cumulant of gaussian noise is zero, we can ignore the expression $C_{pq}(v_k)$ in the continuation of the relations. Equation 12 shows that the cumulant of the time-frequency interfering signals received at the non-cooperative receiver can be separated into the sum of the product of the cumulant and the signal amplitude of each station. This feature will be used in the definition of the amplitude symmetry decision function.

5. AMPLITUDE SYMMETRY DECISION FUNCTION

Deciding on the amplitude symmetry of time-frequency interfering signals received in the non-cooperative receiver can be done by using a mathematical criterion. This decision criterion is developed by assuming the same type of modulations and the duration of symbols and uses the difference in the amplitude of the received signals. Based on Equation 3, the power ratio of the amplitude of the received signals can be defined by

$$P_r = \frac{h_1^2}{h_2^2} \quad (13)$$

If the amplitudes of the two signals are approximately equal to each other, the defined parameter will tend to be one. Therefore, it can be concluded that the amplitudes of the two signals are symmetrical.

$$\lim_{h_1^2 \to h_2^2} P_r \to 1 \quad (14)$$

Also, if the difference between the amplitude of the two signals is significant, so that h_1 can be ignored compared to h_2, for P_r we will have

$$\lim_{h_2^2 \gg h_1^2} P_r \to 0 \quad (15)$$

And if h_2 can be ignored compared to h_1, P_r will tend to infinity

$$\lim_{h_1^2 \gg h_2^2} P_r \to \infty \quad (16)$$

By defining P_r and separating the cumulants of received interfering signals in Equation 12, the decision function can be established. The decision function D with the parameter P_r requires the calculation of a ratio in terms of the even power of h_1 and h_2. Therefore, it is possible to use the ratio of even cumulants C_{2x}, C_{4x} and C_{6x} of the interfering signal y_k and finally make the decision based on thresholding.

According to Equation 12, even cumulants (C_{20}, C_{40}, C_{41}, C_{60}, C_{62}) cannot be used in the decision-making functions, since these cumulants will be complex and affected by phase and frequency offset for the orders of p with q conjugate. Also, according to Table 3, the theoretical values of cumulants C_{20}, C_{41}, C_{60}, and C_{62} for QPSK modulation are equal to zero and cannot be used in the numerator or denominator of ratios. But in cumulants C_{21}, C_{42}, and C_{63}, the effect of phase and frequency offset of interfering signals is eliminated. Therefore, the following cumulant ratios are considered as the proposed decision functions.

$$D_1(P_r) = \left|\frac{C_{42}(y_k)}{C_{21}^2(y_k)}\right| \quad (17)$$

$$D_2(P_r) = \left|\frac{C_{63}(y_k)}{C_{21}^3(y_k)}\right| \quad (18)$$

$$D_3(P_r) = \left|\frac{C_{63}^2(y_k)}{C_{42}^3(y_k)}\right| \quad (19)$$

where |. | indicates absolute value.

By using Equation 12, the cumulants used in the decision functions can be obtained without the effect of phase and frequency offset, so that the product of the amplitude and cumulants C_{21}, C_{42} and C_{63} of $x_k{}^{(1)}$ and $x_k{}^{(2)}$ signals are separated as follows

$$\begin{aligned} C_{21} &= h_1^2 C_{21}\left(x_k{}^{(1)}\right) + h_2^2 C_{21}\left(x_k{}^{(2)}\right) \\ &= h_2^2\left[P_r C_{21}\left(x_k{}^{(1)}\right) + C_{21}\left(x_k{}^{(2)}\right)\right] \end{aligned} \quad (20)$$

$$\begin{aligned} C_{42} &= h_1^4 C_{42}\left(x_k{}^{(1)}\right) + h_2^4 C_{42}\left(x_k{}^{(2)}\right) \\ &= h_2^4\left[P_r^2 C_{42}(x_k{}^{(1)}) + C_{42}(x_k{}^{(2)})\right] \end{aligned} \quad (21)$$

$$\begin{aligned} C_{63} &= h_1^6 C_{63}(x_k{}^{(1)}) + h_2^6 C_{63}(x_k{}^{(2)}) \\ &= h_2^6\left[P_r^3 C_{63}(x_k{}^{(1)}) + C_{63}(x_k{}^{(2)})\right] \end{aligned} \quad (22)$$

By placing Equations 20 into 22 inside Equations 17 into 19, the following theoretical results will be obtained in terms of the parameter P_r for the decision-making functions:

$$\begin{aligned} D_1(P_r) &= \left|\frac{C_{42}(y_k)}{C_{21}^2(y_k)}\right| \\ &= \left|\frac{P_r^2 C_{42}(x_k{}^{(1)}) + C_{42}(x_k{}^{(2)})}{(P_r C_{21}(x_k{}^{(1)}) + C_{21}(x_k{}^{(2)}))^2}\right| \end{aligned} \quad (23)$$

$$\begin{aligned} D_2(P_r) &= \left|\frac{C_{63}(y_k)}{C_{21}^3(y_k)}\right| \\ &= \left|\frac{P_r^3 C_{63}(x_k{}^{(1)}) + C_{63}(x_k{}^{(2)})}{(P_r C_{21}(x_k{}^{(1)}) + C_{21}(x_k{}^{(2)}))^3}\right| \end{aligned} \quad (24)$$

$$\begin{aligned} D_3(P_r) &= \left|\frac{C_{63}^2(y_k)}{C_{42}^3(y_k)}\right| \\ &= \left|\frac{\left(P_r^3 C_{63}(x_k{}^{(1)}) + C_{63}(x_k{}^{(2)})\right)^2}{(P_r^2 C_{42}(x_k{}^{(1)}) + C_{42}(x_k{}^{(2)}))^3}\right| \end{aligned} \quad (25)$$

According to equations 23 to 25, the amplitude symmetry will occur when P_r tends to one. Therefore, the decision functions will tend to the theoretical values of Table 4.

Table 4. Theoretical values of decision-making functions in the case of symmetric amplitude.

	$P_r \to 1$
D_1	$\left\|\frac{C_{42}(x_k{}^{(1)}) + C_{42}(x_k{}^{(2)})}{(C_{21}(x_k{}^{(1)}) + C_{21}(x_k{}^{(2)}))^2}\right\|$
D_2	$\left\|\frac{C_{63}(x_k{}^{(1)}) + C_{63}(x_k{}^{(2)})}{(C_{21}(x_k{}^{(1)}) + C_{21}(x_k{}^{(2)}))^3}\right\|$
D_3	$\left\|\frac{\left(C_{63}(x_k{}^{(1)}) + C_{63}(x_k{}^{(2)})\right)^2}{(C_{42}(x_k{}^{(1)}) + C_{42}(x_k{}^{(2)}))^3}\right\|$

Also, amplitude asymmetry will occur when P_r tends to zero or infinity. Therefore, in this case, the decision functions will tend to the theoretical values of the Table 5.

Table 5. Theoretical values of decision-making functions in the case of asymmetric amplitude.

	$P_r \to 0$	$P_r \to \infty$
D_1	$\left\|\frac{C_{42}(x_k{}^{(2)})}{(C_{21}(x_k{}^{(2)}))^2}\right\|$	$\left\|\frac{C_{42}(x_k{}^{(1)})}{(C_{21}(x_k{}^{(1)}))^2}\right\|$
D_2	$\left\|\frac{C_{63}(x_k{}^{(2)})}{(C_{21}(x_k{}^{(2)}))^3}\right\|$	$\left\|\frac{C_{63}(x_k{}^{(1)})}{(C_{21}(x_k{}^{(1)}))^3}\right\|$
D_3	$\left\|\frac{\left(C_{63}(x_k{}^{(2)})\right)^2}{(C_{42}(x_k{}^{(2)}))^3}\right\|$	$\left\|\frac{\left(C_{63}(x_k{}^{(1)})\right)^2}{(C_{42}(x_k{}^{(1)}))^3}\right\|$

In practice, it is not possible to use the theoretical values of the decision functions of interfering signals to decide the amplitude symmetry, since P_r is unknown due to interference. Therefore, the calculation of the values of the decision functions is done only by using a sufficiently long sequence of time-frequency interfering signals samples received in the non-cooperative receiver, and the values of cumulants in these functions are calculated by the following simple estimates [22]:

$$\hat{C}_{20} = \frac{1}{N}\sum_{k=1}^{N} y^2(k) \quad (26)$$

$$\hat{C}_{21} = \frac{1}{N}\sum_{k=1}^{N} |y(k)|^2 \quad (27)$$

$$\hat{C}_{42} = \frac{1}{N}\sum_{k=1}^{N} |y(k)|^4 - \left|\hat{C}_{20}\right|^2 - 2\hat{C}_{21}^2 \quad (28)$$

$$\hat{C}_{63} = \frac{1}{N}\sum_{k=1}^{N} |y(k)|^6 - 9\hat{C}_{21}\hat{C}_{42} - 6\hat{C}_{21}^3 \quad (29)$$

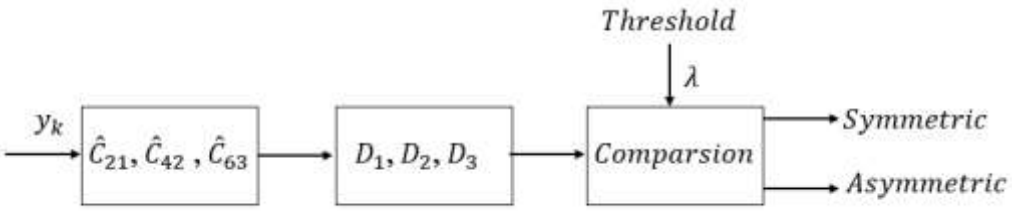

Fig. 5. Block diagram of the proposed method for amplitude symmetry decision.

Therefore, according to the block diagram in Figure 4, the proposed method begins with the calculation and estimation of the desired cumulants from the received time-frequency interfering signal and after calculating the values of the decision functions, it detects the symmetry or asymmetry from the comparison with the determined threshold.

6. SIMULATION RESULTS

The Equations 17 to 19 of the decision functions proposed are used in [16], [22], and [23] as feature-based methods in the classification of digital modulations. By comparing and evaluating the results of simulated data, the appropriate decision function can be selected.

6.1. Comparison of theoretical and simulation results

In this part, theoretical and simulated values of decision-making functions are investigated. The theoretical values include the data results from the mathematical expressions on the right side of the decision functions of Equations 24 to 26. The simulation values also include the data results from the mathematical expressions on the left side of the decision functions 24 to 26, for which the Equations 27 to 29 should be used for calculation.

The simulation data is generated from the time-frequency combination of two signals with the same modulations, both of BPSK or QPSK type. In addition to having the same parameters, the two signals also pass through the same shaping filters. The difference between the two interfering signals is only in the phase offsets, frequency offsets and amplitude, so the power levels of the amplitudes differ from -20dB to +20dB. P_r shows the power level difference of the amplitudes in Figures 6 to 8 with. In this experiment, the effect of noise is ignored.

Figures 6 to 8 show that with the increase of P_r(the power level difference of the amplitudes), from -20dB for both BPSK and QPSK interfering signals, the values of decision functions decrease in the theoretical and simulation values. The results of these functions reach their minimum when the power level difference of the amplitudes is zero and the two interfering signals are completely symmetric. Again, with the increase of P_r, the results of these functions also increase. Figures clearly show that the values of functions D_1, D_2 and D_3 using the theoretical values and simulation have the same behavior for different values of the power level difference, and the results of the simulation values can be used instead of the theoretical values. The results of these decision-making functions in terms of P_r show well that if the amplitude of the time-frequency interfering signals is completely symmetric, the values of these three functions are at their minimum, and in this case, the symmetry of the amplitudes can be concluded and with increasing the amplitude level difference and moving away from the minimum value, the amplitude asymmetry of the interfering signals is concluded.

The results of the decision functions in the power level difference of -20dB and +20dB are very close to each other and confirm the results of Table 5.

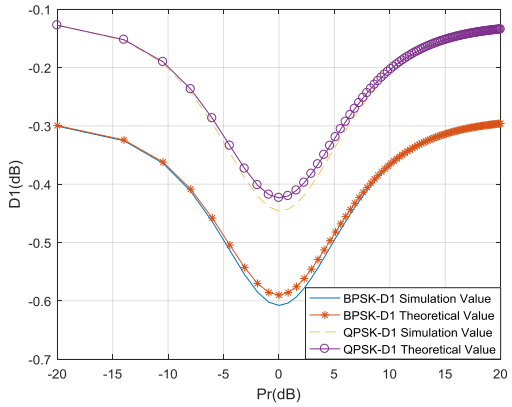

Fig. 6. The theoretical and simulated values of the decision function D_1 according to the difference in the power level of the amplitude of two time-frequency interfering signals, BPSK and QPSK.

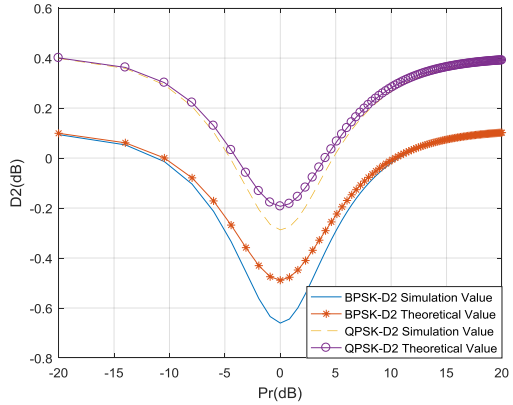

Fig. 7. Theoretical and simulated values of the decision function D_2 according to the difference in the power level of the amplitude of two time-frequency interfering signals BPSK and QPSK.

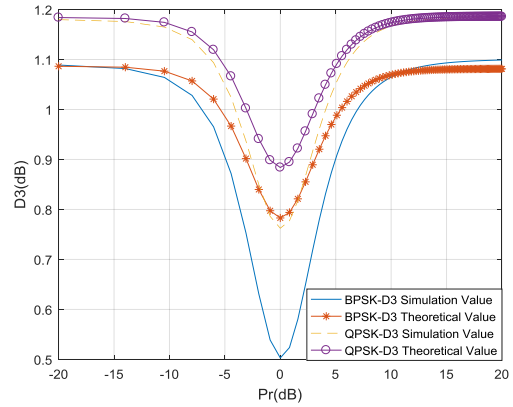

Fig. 8. Theoretical and simulated values of the decision function D_3 according to the difference in the power level of the amplitude of two time-frequency interference signals BPSK and QPSK.

6.2. Comparison of decision functions in the symmetric mode

In this part we examine and compare the ability of decision functions to identify the amplitude symmetry mode at different signal-to-noise-ratio values. For this purpose, 100 time-frequency interfering signals with symmetric amplitudes have been used in each SNR value that ranges from -20dB to +20dB. For all interfering signals, which are either BPSK or QPSK, the values of the decision functions have been calculated and shown as a blue dot in Figure 9. The red line shows the average values of the blue points at the same SNR.

In all Figures, the values of decision functions have a large variance (blue dot) at the signal-to-noise-ratio of less than zero. So, it is not possible to obtain a favorable result about the symmetry of amplitude. But as the signal-to-noise increases from zero, the accuracy of decisions about amplitude symmetry increases and gets closer to the uniform line (red line). therefore, it can be used for thresholding and the final decision on the symmetry or asymmetry of the amplitudes.

The variance of the function's value for the signal-to-noise-ratio greater than zero is shown in Table 6. This Table shows that the lowest variance value is associated with D_3. Therefore, it can be concluded that this decision function is more stable compared to the other two.

Table 6. Variance values of decision functions in the case of symmetric amplitude.

	D_1	D_2	D_3
BPSK	0.0263	0.0637	0.0100
QPSK	0.0252	0.0457	0.0099

6.3. Probability of correct classification

In this part, decision functions based on the probability of correct classification of time-frequency interfering signals in terms of amplitude symmetry or asymmetry are investigated and compared. For this purpose, 5000 interfering signal samples have been used in the form of Monte Carlo. The signal-to-noise-ratio varies from 0dB to 25dB. The probability of correct classification is defined as follows:

$$P_{CC} = \sum_{k=1}^{2} P(y_c|y_t)\, P_k \tag{30}$$

where P_k is the probability of the symmetric amplitude and since the number of symmetric and asymmetric signals is considered equal, $P_k = \frac{1}{2}$. $P(y_c|y_t)$ is the conditional probability of correct classification of the received signal when the amplitude of the transmitted signals is symmetric or asymmetric. Figures 10 and 11 show the probability of correct classification of each decision function for BPSK and QPSK, respectively.

These Figures show that the probability of correct classification of interfering signals increases with the increase of the signal-to-noise-ratio. Comparing the charts shows that among the decision functions, D_3 is more successful at all signal-to-noise-ratio values. Also, in the signal-to-noise range of less than 5dB, decision functions D_1 and D_2 have a low probability of correct

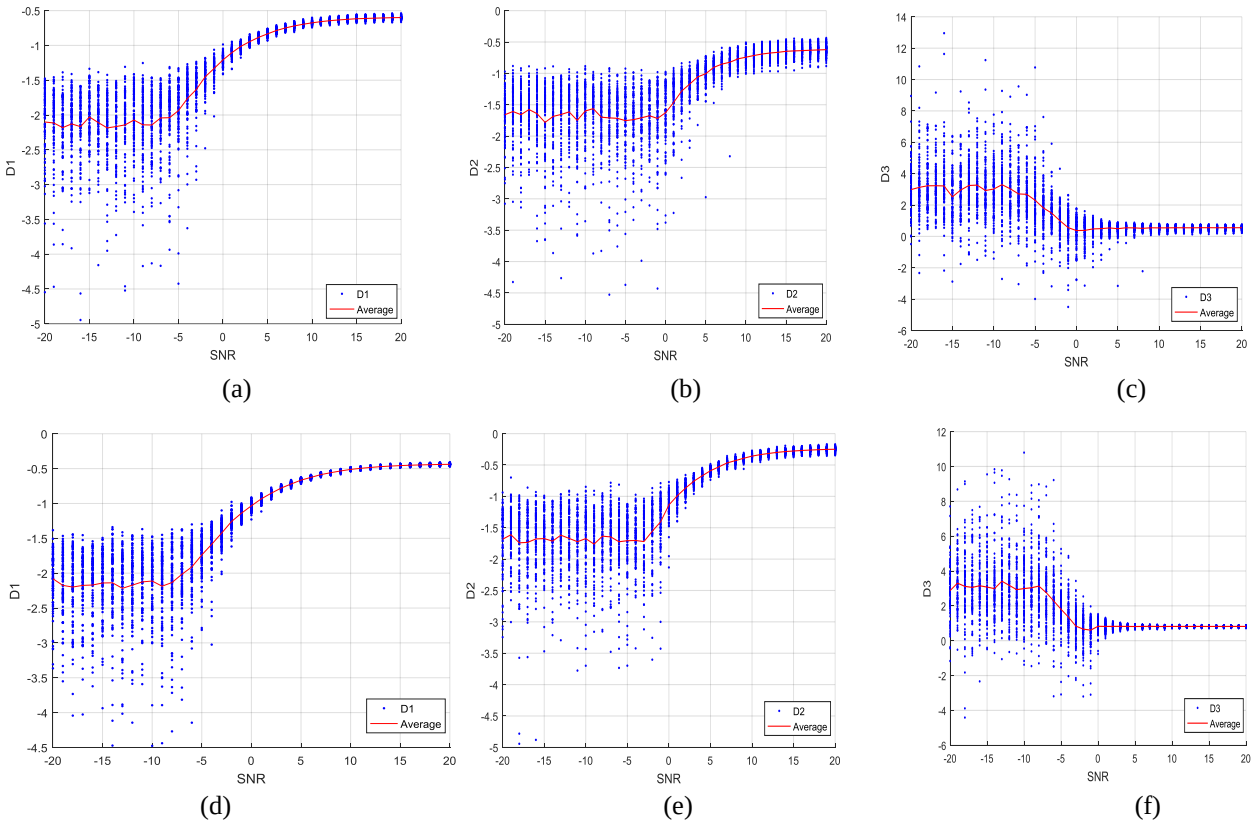

Fig. 9. Values of decision functions D_1, $D_2$and $D_3$for interference signals with amplitude symmetric at different signal-to-noise levels (a) BPSK-D1 (b) BPSK- D2 (c) BPSK-D3 (d) QPSK-D1 (e) QPSK-D2 (f) QPSK-D3.

classification. Comparing the two charts in terms of the type of modulations shows that the probability of correct classification in time-frequency interfering signals with QPSK modulation is higher than with BPSK modulation.

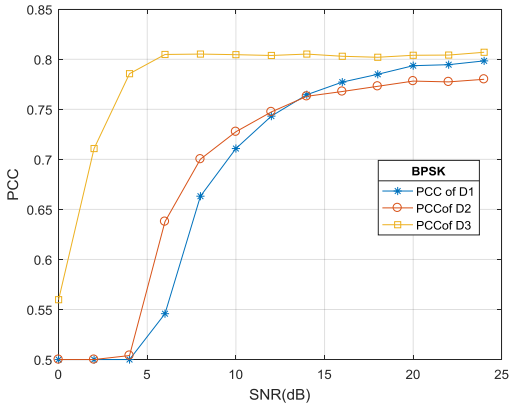

Fig. 10. Probability of correct classification of BPSK time-frequency interfering signal.

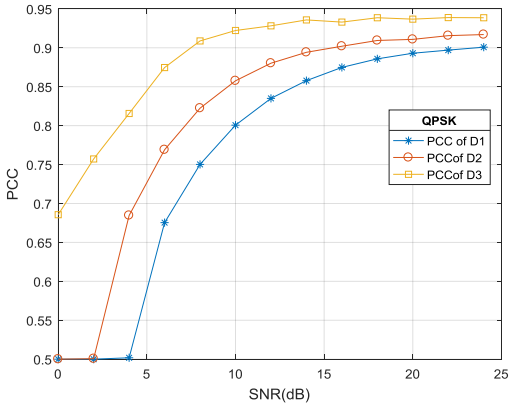

Fig. 11. Probability of correct classification of QPSK time-frequency interfering signal.

7. CONCLUSION

The separation of interfering time-frequency signals of CNC satellite communications is one of the complex issues. Researchers have proposed methods to separate these signals. These methods are affected by the symmetry or asymmetry of the amplitude of time-frequency interfering signals. So far, no approach is provided to detect symmetry in these signals. For this reason, higher-order statistics, which

are resistant to noise and rotation of the signal, have been used in this article. After developing the cumulant relations on the mathematical model of the received signal in the non-cooperative receiver, the cumulant ratios are used to define the decision functions about the symmetry of the interfering signal amplitude. The decision functions were compared in terms of theoretical and simulation values. It was found that simulation values can be used instead of theoretical values. Also, these functions were compared in terms of different signal-to-noise levels and the probability of correct classification. The comparison and evaluations show that the decision-making function based on the sixth and fourth ratio cumulants has more reliability. Simulation results show that the probability of correct classification with this function at higher than 25dB signal-to-noise-ratio for BPSK modulation is more than 80%, and for QPSK modulation is more than 90%.

REFERENCES

[1] Y. Yang, H. Peng, D. Zhang and X. Dai, **"Markov Chain Monte Carlo-Based Separation of Paired Carrier Multiple Access Signals,"** *IEEE Communications Letters* , vol. 20, no. 11, pp. 2209 - 2212, 2016.

[2] S. Preethi and k.Rajeswari, **"A Survey on Multiple Access Techniques for Mobile communication,"** *International Journal of Emerging Trends & Technology in Computer Science (IJETTCS)*, vol. 1, pp. 1-5, 2015.

[3] C. Agne, M. B. Cornell, M. Dale, R. Kearns and F. Lee, **"Shared-spectrum bandwidth efficient satellite communications,"** in *2010 - MILCOM 2010 MILITARY COMMUNICATIONS CONFERENCE*, San Jose, CA, USA, 2010.

[4] Y. Guo, H. Peng and J. Fu, **"Joint Blind Parameter Estimation of Non-cooperative High-Order Modulated PCMA Signals,"** *KSII Transactions on Internet and Information Systems (TIIS)*, vol. 12, no. 10, pp. 4873-4888 , 2018.

[5] Q. Deng, S. Zhang, G. Chen and H. Lu, **"Blind separation of noncooperative paired carrier multiple access signals based on improved quantum- inspired evolutionary algorithm and receding horizon optimization,"** *Concurrency Computat Pract Exper*, vol. 34, 2021.

[6] L. Brnak, M. Svarc, V. Platenka and M. Richterova, **"Blind Equalization of Carrier in Carrier Signals by Using Adaptive Filters,"** in *2018 New Trends in Signal Processing (NTSP)*, Slovakia, 2018.

[7] P.-h. Mo, X.-x. Fan and L. You**, "A novel and blind detection scheme for asymmetric PCMA system,"** in *Proceedings of 2013 3rd International Conference on Computer Science and Network Technology*, Dalian, China, 2013.

[8] C. Peng, X. Yang and Y. Zhang, **"Blind separation of asymmetric signals based on Synchrosqueezing Wavelet Transform,"** *MATEC Web of Conferences*, vol. 232, 2018.

[9] Y. Yang, D. Zhang and H. Peng, **"Frequency Offset Estimation of the Linear Mixture of Two Co-Frequency 8 Phase-Shift Keying Modulated Signals,"** *IET Signal Processing*, vol. 9, no. 2, pp. 186-192, 2015.

[10] Y. Yang, H. Peng, D. Zhang and P. Wang, **"Iterative Processing Structure for the Single-Channel Mixture of Digital-Modulated Adjacent-Frequency Source Signals,"** *IEEE Transactions on Vehicular Technology*, vol. 69, no. 2, pp. 1639 - 1650, 2020.

[11] X. Liu, Y. L. Guan, S. N. Koh, Z. Liu and P. Wang, **"Low-Complexity Single-Channel Blind Separation of Co-Frequency Coded Signals,"** *IEEE Communications Letters*, vol. 22, no. 5, pp. 990 - 993, 2018.

[12] W. Chi, P. Hua and F. Junhui, **"A Blind Separation Method of PCMA Signals Based on MSGibbs Algorithm,"** *Journal of Physics: Conference Series*, vol. 1168, no. 5, 2019.

[13] C. Wei, H. Peng and J. Fan, **"Single-channel Demodulation Algorithm for Non-cooperative PCMA Signals Based on Neural Network,"** *KSII Transactions on Internet and Information Systems*, vol. 13, no. 7, pp. 3433-3446, 2019.

[14] M. Dankberg, **"Paired Carrier Multiple Access For Satellite Communication,"** in *In 17th AIAA International Communications Satellite Systems Conference and Exhibit*, Honolulu, Hawaii, 1998.

[15] Y. Liang, X. Xiang, Y. Sun, X. Da, C. Li and L. Yin, **"Novel Modulation Recognition for WFRFT-Based System Using 4th-Order Cumulants,"** *IEEE Access* , vol. 7, pp. 86018 - 86025, 2019.

[16] M. S. Pajic, M. Veinovic, M. Peric and V. D. Orlic, **"Modulation Order Reduction Method for Improving the Performance of AMC Algorithm Based on Sixth–Order Cumulants,"** *IEEE Access* , vol. 8, pp. 106386 - 106394, 2020.

[17] T. Li, Y. Li and O. A. Dobre, **"Modulation Classification Based on Fourth-Order Cumulants of Superposed Signal in NOMA Systems,"** *IEEE Transactions on Information Forensics and Security* , vol. 16, pp. 2885 - 2897, 2021.

[18] A. Abdelmutalab, K. Assaleh and M. El-Tarhuni, **"Automatic modulation classification based on high order cumulants and hierarchical polynomial classifiers,"** *Physical Communication*, vol. 21, pp. 10-18, 2016.

[19] Z. Ge, H. Jiang, Y. Guo and J. Zhou, **"Accuracy Analysis of Feature-Based Automatic Modulation Classification via Deep Neural Network,"** *Sensors*, vol. 21, 2021.

[20] H. Ochiai, **"High-Order Moments and Gaussianity of Single-Carrier and OFDM**

Signals," *IEEE Transactions on Communications* , vol. 63, no. 12, pp. 4964 - 4976, 2015.

[21] A. Swami and B. M. Sadler, **"Hierarchical digital modulation classification using cumulants,"** *IEEE Transactions on Communications* , vol. 48, no. 3, pp. 416 - 429, 2000.

[22] F. Liu, Z. Zhang and R. Zhou, **"Automatic Modulation Recognition Based on CNN and GRU,"** *Tsinghua Science and Technology*, vol. 27, no. 2, pp. 422 - 431, 2022.

[23] M. SIMIC and M. S. :. D. ORLIC, **"Automatic Modulation Classification of Real Signals in AWGN Channel Based on Sixth-Order Cumulants,"** *Radioengineering*, vol. 30, no. 1, pp. 204-214, 2021.